AIP | Applied Physics Letters

Mapping the electronic properties of individual graphene grain boundaries

Levente Tapasztó, Péter Nemes-Incze, Gergely Dobrik, Kwon Jae Yoo, Chanyong Hwang et al.

Citation: Appl. Phys. Lett. **100**, 053114 (2012); doi: 10.1063/1.3681375
View online: http://dx.doi.org/10.1063/1.3681375
View Table of Contents: http://apl.aip.org/resource/1/APPLAB/v100/i5
Published by the American Institute of Physics.

Mapping the electronic properties of individual graphene grain boundaries

Levente Tapasztó,[1,2,a)] Péter Nemes-Incze,[1,2] Gergely Dobrik,[1,2] Kwon Jae Yoo,[2,3] Chanyong Hwang,[2,3] and László P Biró[1,2]
[1]*Research Institute for Technical Physics and Materials Science, P.O. Box 49, 1525 Budapest, Hungary*
[2]*Korea-Hungary Joint Laboratory for Nanosciences, P.O. Box 49, 1525 Budapest, Hungary*
[3]*Center for Advanced Instrumentation, Division of Industrial Metrology, Korea Research Institute of Standards and Science, Yuseong, Daejeon 305-340, South Korea*

(Received 9 November 2011; accepted 12 January 2012; published online 1 February 2012)

Grain boundaries, the characteristic topological defects of chemical vapor deposition grown graphene samples, are expected to substantially alter the electronic properties of the unperturbed graphene lattice. However, there is very little experimental insight into the underlying mechanisms. Here, we systematically map the electronic properties of individual graphene grain boundaries by scanning tunneling microscopy and spatially resolved tunneling spectroscopy measurements. The tunneling spectroscopy data reveal that the conductivity inside the boundaries is markedly suppressed for both electron and hole-type charge carriers. Furthermore, graphene grain boundaries can give rise to n-type inversion channels within the p-doped graphene sheets, forming p-n junctions with sharp interfaces on the nanometer scale. These properties persist for grain boundaries of various configurations and are robust against structural disorder. © *2012 American Institute of Physics*. [doi:10.1063/1.3681375]

Grain boundaries (GBs) of the two-dimensional graphene lattice are topological line-defects consisting of non-hexagonal carbon rings as evidenced by aberration corrected high resolution TEM investigations.[1] They are ubiquitous in graphene samples grown by chemical vapor deposition (CVD) and are expected to further enrich the unique electronic properties of the defect-free graphene lattice.[2,3] The CVD synthesis method and consequently dealing with grain boundaries are also of high practical relevance, as it allows the growth of wafer-scale continuous single layer samples.[4] However, a fundamental challenge of this technique is that the electrical quality (conductivity, charge carrier mobility) of the as-grown graphene samples falls behind by about an order of magnitude as compared to mechanically exfoliated graphene.[3,5] There is growing evidence that the presence of grain boundaries is responsible for the degradation of the intrinsic electronic performance of these samples.[2,3,6] In a simple qualitative picture, the defective grain boundaries can be perceived as structural barriers impeding the propagation of the charge carriers. However, very little is known about the underlying mechanism, which is of particular importance in our efforts towards understanding and ultimately controlling electronic transport in the presence of GBs.

In this work, we employ local probe methods, namely, scanning tunneling microscopy (STM) and spectroscopy (STS) measurements, which allow us to locally explore the electronic behavior of individual graphene grain boundaries at the nanometer scale.

The graphene samples used in this study have been prepared by the CVD technique, known to yield polycrystalline samples with a relatively high density of grain boundaries.[1,4,7] Copper single crystal substrates as well as polycrystalline copper foils have been introduced into a furnace and annealed at 990 °C in hydrogen atmosphere (2 sccm) for 30 min. The graphene was grown by letting in CH_4 gas (35 sccm) for 1 min. Afterwards the system was cooled down to room temperature at a cooling rate of 50 K/min. The presence of a continuous graphene single layer covering the surface of the copper substrate after the growth was verified by Raman spectroscopy. Scanning tunneling microscopy and spectroscopy measurements have been performed on the as-grown samples under ambient conditions, without any further processing (e.g., transfer or electrode patterning).

As can be seen from Fig. 1, the grain boundaries of graphene can be identified in the STM images as linear

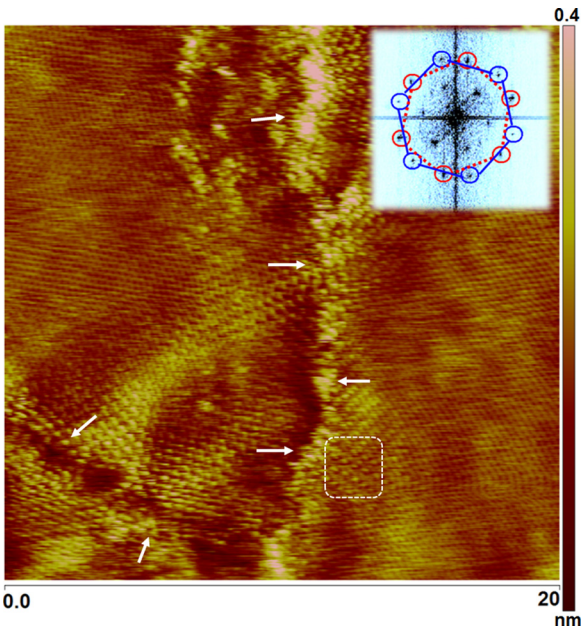

FIG. 1. (Color online) Atomic resolution STM image (50 mV, 1 nA) of CVD graphene on Cu substrate revealing linear defective features corresponding to grain boundaries. The square in the vicinity of the GB marks the presence of electronic superstructures. Inset: FT STM image displaying two hexagons rotated by 25° corresponding to the difference in the orientation of the left and the right grain.

[a)]Author to whom correspondence should be addressed. Electronic mail: tapaszto@mfa.kfki.hu.

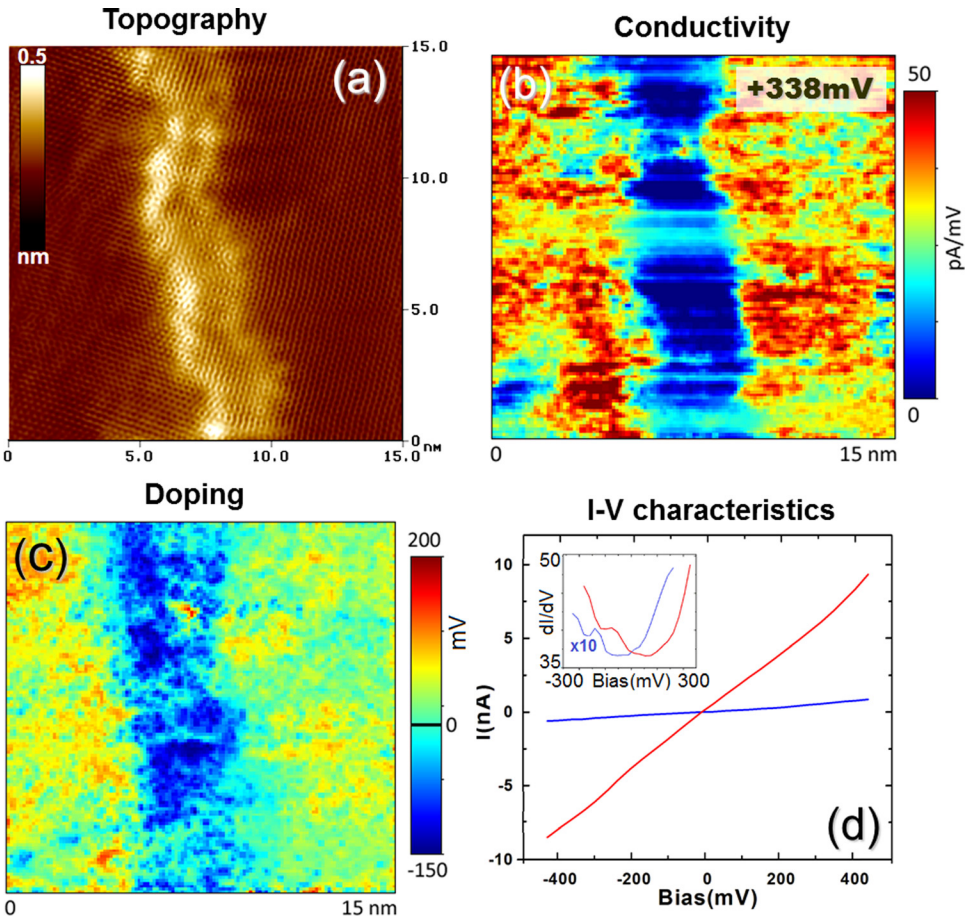

FIG. 2. (Color online) (a) Atomic resolution constant current topographic STM image (100 mV, 1 nA) of a 29° graphene grain boundary, with the boundary region displaying a bright contrast. (b) Spatially resolved tunneling conductivity map revealing a markedly suppressed conductivity at the grain boundary region. (c) Spatial map of the Dirac-point position relative to the Fermi energy, indicating the local doping. (d) Representative individual current-voltage characteristics acquired at the grain boundary (low, blue) and over the unperturbed graphene lattice (steep, red). The corresponding numerical derivatives (differential conductance) are shown in the inset.

defective features perturbing the hexagonal graphene lattice along more or less straight lines. They can appear both in light and dark contrast resulting from the complex interplay between the topography and electronic properties of the GB as well as the STM imaging conditions. Atomic resolution images reveal that indeed the crystallographic orientations of the honeycomb lattices on the two sides of such a line-defect are rotated relative to each other confirming the tilt nature of the grain boundary. The GB angle can be determined either in direct space or much more conveniently by generating the Fourier-transformed (FT) image (inset of Fig. 1). The angle of rotation between the two hexagons in the FT image gives the tilt angle of the boundary connecting the left and the right grain in Fig. 1. For this particular boundary, the tilt angle was found to be $\theta = 25°$.

A closer examination of the STM image in Fig. 1 reveals the presence of superstructures in the vicinity of the GBs (e.g. marked by the white square). These superstructures can be understood considering the scattering and interference of the charge carriers on the defective grain boundary region,[8,9] revealing that the dominant scattering mechanism at graphene grain boundaries is the short-range, inter-valley scattering. This finding is in good agreement with a recent experimental work reporting the observation of prominent weak localization in electronic transport through individual graphene grain boundaries, which also identifies grain boundaries as the primary source of inter-valley scattering in graphene.[3,6]

In Fig. 2(a), a 29° grain boundary is shown in atomic resolution, displaying a bright contrast along the boundary region. In contrast to HR-TEM imaging, the exact atomic structure of the GB cannot be directly resolved in atomic resolution STM images since local electronic effects distort the atomic picture at the GB.[10–12] However, this drawback is also one of the biggest advantages of this method, allowing access to study the electronic properties of the GBs. In order to achieve this, we have performed spatially resolved tunneling spectroscopy on individual graphene grain boundaries. In this operation mode, individual tunneling I-V characteristics are acquired with the tip fixed over a specific location of the sample and the sample voltage ramped within a given window while measuring the corresponding tunnel current. During the mapping, the STM tip is moved between adjacent I-V measurement locations by keeping the tip-height (z-position) constant with a good approximation. The constant height measurement mode (instead of constant current) allows us to directly compare the conductivity of the grain boundary with the defect-free graphene areas. Fig. 2(b) shows the tunneling conductivity map obtained by plotting the numerical derivative of each individual current-voltage characteristic plotted at $V_{bias} = +338$ mV. From the map in Fig. 2(b), it is apparent that the conductivity is markedly suppressed at the grain boundary within a region of a few nanometers. This behavior persists upon changing the polarity of the sample bias, indicating that the conductivity is suppressed for both electron and holetype charge carriers.

Individual current voltage characteristics of the two regions are shown in Fig. 2(d). It is apparent that the

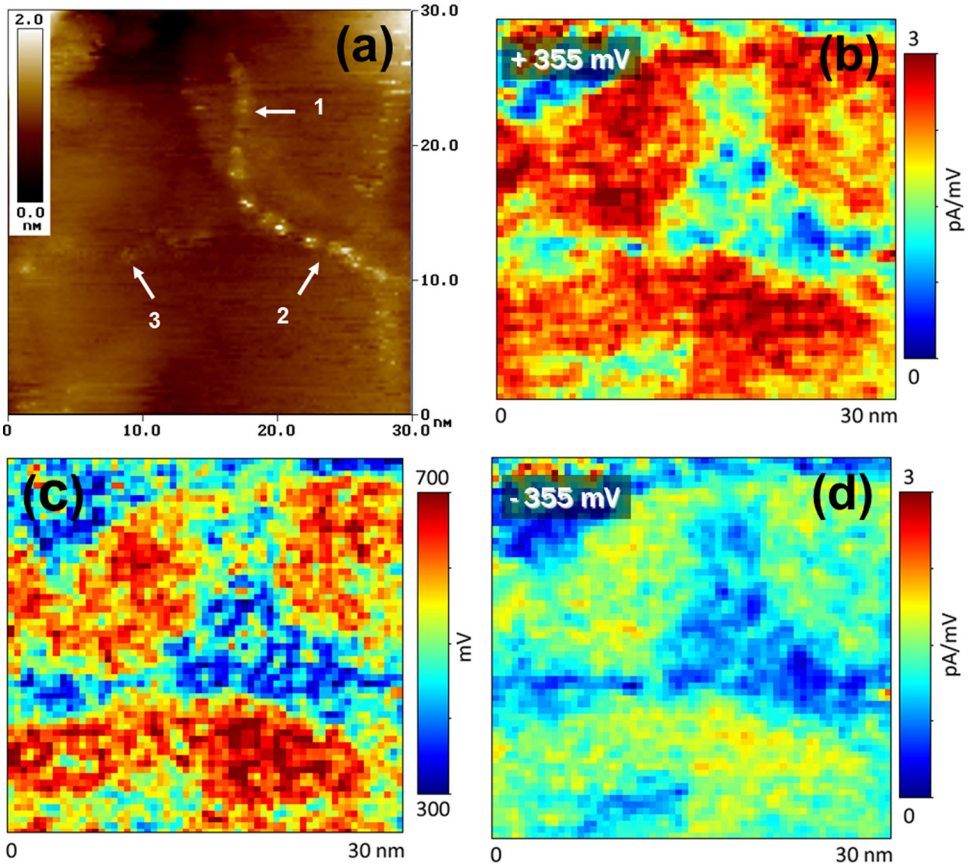

FIG. 3. (Color online) (a) STM image (100 mV, 2 nA) of a graphene grain boundary triple junction consisting of three grain boundaries with relative angles of 27°, 21°, and 12°. (b) Local conductivity map showing the suppression of conductivity on all grain boundaries for positive (b) and negative sample bias (d). (c) Local doping map displaying a substantially reduced p-doping all over the GB triple junction region.

conductivity within the grain boundary is about an order of magnitude lower as compared to the defect-free graphene lattice. This implies that from the electrical point of view, the interconnected GB network divides the graphene sample into highly conductive single crystalline islands delimited by more resistive interface regions of a few (3-5) nanometer widths. These findings are in agreement with transport measurements reporting that the inter-grain conductivity (across a GB) was found to be reduced by approximately an order of magnitude as compared to the intra grain conductivity (no GB).[3,6]

We have also mapped the spatial distribution of the tunneling conductivity (LDOS) minima position. Since our tunneling spectra show no signature of gap-like features,[13] the conductivity minima is expected to correlate with the position of the Dirac point.[14–16] The position of the Dirac point relative to the Fermi energy (zero bias) is indicative of the local doping.[15,17] A striking difference has been revealed in the position of the Dirac point at the grain boundaries and over the defect free graphene lattice, as apparent form Fig. 2(c). The unperturbed graphene lattice was found to be p-doped (Dirac point at +100 mV, corresponding to a hole density of about $7 \times 10^{11}\,\mathrm{cm}^{-2}$) in agreement with various transport measurements on CVD grown graphene samples under ambient conditions.[3,17] By contrast, at the grain boundaries, the Dirac point is located around −80 mV, corresponding to a pronounced n-doping of $5 \times 10^{11}\,\mathrm{cm}^{-2}$. According to these results, the GBs of CVD graphene form n-doped inversion channels within the overall p-doped graphene lattice. The origin of this phenomenon can be attributed to the self doping, whereupon a charge transfer occurs between the defect-free graphene lattice and the non-hexagonal carbon rings making up the grain boundary.[18,19] An additional source of doping could come from functional groups or adsorbates, which preferentially attach to the defective grain boundaries. Regardless of the doping source, the inversion channels introduce a series on *p-n-p* junctions in the polycrystalline graphene samples. The presence of these inversion channels and p-n junctions can be exploited in various applications, opening the way towards designing nanoelectronic devices based on graphene grain boundaries. In the p-n junctions created so far by chemical doping[20] or electrostatic dual gating,[21] the carrier concentration changed smoothly on the nano-scale (even up to micro-scale), while in the case of graphene grain boundaries reported here, the doping profile changes abruptly within a few nanometers. Sharp, step-like p-n interfaces in graphene are of great importance as they are required for the experimental study of several intriguing phenomena, such as Klein tunneling[22] and could make feasible the realization of a series of devices, from Veselago lenses[23] to electronic waveguides,[24] which were experimentally inaccessible so far.

Moreover, the above findings of suppressed conductivity and local-doping have been confirmed for several individual grain boundaries with various tilt angles (atomic structure) and grown on different substrates (Cu single crystal, Cu foil). This evidences that the above reported electronic properties of graphene grain boundaries are quite universal and robust, which is somehow in contrast with the theoretical expectations predicting that the properties of GBs sensitively depend on their precise atomic structure.[2] The reason for this apparent discrepancy is probably due to the fact that theoretical works model GBs as periodic arrays of dislocations,

while the experimentally investigated grain boundaries are usually neither straight nor periodic and contain a significant amount of disorder.

In order to illustrate the universal nature and robustness of the observed electronic behavior of graphene GBs in Fig. 3, we show a grain boundary triple junction consisting of three distinct grain boundaries with tilt angles of 27°, 21°, and 12°. As can be seen the conductivity maps and doping profiles are quite similar for all three GBs, underscoring the universal character of the reported phenomena. Here, we note that the intensity of self doping is not always sufficient to introduce an inversion channel (p-n-p junction) often it only gives rise p-p'-p junctions, where $p > p'$.

These findings shed some light on the origin of the electronic behavior of graphene grain boundaries and could open the way towards the realization of a series of devices exploiting the grain boundaries for tailoring the electronic transport in graphene at the nano-scale.

This work has been conducted within the framework of the Joint Korean-Hungarian Laboratory for Nanosciences (JKHLN), the Converging Research Center Program through the Ministry of Education, Science and Technology (2010K000980), OTKA grant PD 84244 and K 101599.

[1]P. Y. Huang, C. S. Ruiz-Vargas, A. M. van der Zande, W. S. Whitney, M. P. Levendorf, J. W. Kevek, S. Garg, J. S. Alden, C. J. Hustedt, Y. Zhu *et al.*, Nature **469**, 389 (2011).
[2]O. V. Yagzev and S. G. Louie, Nature Mater. **9**, 806 (2010).
[3]Q. Yu, L. A. Jauregui, W. Wu, R. Colby, J. F. Tian, Z. H. Su, H. L. Cao, Z. H. Liu, D. Pandey, D. G. Wei *et al.*, Nature Mater. **10**, 443 (2011).
[4]X. S. Li, W. W. Cai, J. H. An, S. Kim, J. Nah, D. X. Yang, R. Piner, A. Velamakanni, I. Jung, E. Tutuc *et al.*, Science **324**, 1312 (2009).
[5]K. S. Kim, Y. Zhao, H. Jang, S. Y. Lee, J. M. Kim, K. S. Kim, J. H. Ahn, P. Kim, J. Y. Choi, and B. H. Hong, Nature **457**, 706 (2009).
[6]L. A. Jaregui, H. Cao, W. Wu, Q. Yu, and Y. P. Chen, Solid State Commun. **151**, 1100 (2011).
[7]P. Nemes-Incze, K. J. Yoo, L. Tapaszto, G. Dobrik, J. Labar, Z. E. Horvath, C. Hwang, and L. P. Biro, Appl. Phys. Lett. **99**, 023104 (2011).
[8]H. A. Mizes and J. S. Foster, Science, **244**, 559 (1989).
[9]L. Tapaszto, G. Dobrik, P. Nemes-Incze, G. Vertesy, P. Lambin, and L. P. Biro, Phys. Rev. B **78**, 233407 (2008).
[10]P. Simonis, C. Goffaux, P. A. Thiry, L. P. Biro, P. Lambin, and V. Meunier, Surf. Sci. **511**, 319 (2002).
[11]J. Cervenka and C. F. J. Flipse, Phys. Rev. B **79**, 195429 (2009).
[12]W. H. Brito, R. Kagimura, and R. H. Miwa, Appl. Phys. Lett. **98**, 213107 (2011).
[13]J. Zhang, V. W. Brar, F. Wang, C. Girit, Y. Yayon, M. Panlasigui, A. Zettl, and M. F. Crommie, Nat. Phys. **4**, 627 (2008).
[14]J. Xue, J. Sanchez-Yamagishi, D. Bulmash, P. Jacquod, A. Deshpande, K. Watanabe, T. Taniguchi, P. Jarillo-Herrero, and B. J. Leroy, Nature Mater. **10**, 282 (2011).
[15]G. Li, A. Luican, and E. Y. Andrei, Phys. Rev. Lett. **102**, 176804 (2009).
[16]A. Deshpadne, W. Bao, F. Miao, C. N. Lau, and B. J. LeRoy, Phys. Rev. B **79**, 205411 (2009).
[17]H. Cao, Y. Qingkai, L. A. Jauregui, J. Tian, W. Wu, Z. Liu, R. Jalilian, D. K. Benjamin, Z. Jiang, J. Bao *et al.*, Appl. Phys. Lett. **96**, 122106 (2010).
[18]N. M. R. Peres, F. Guinea, and A. H. Castro Neto, Phys. Rev. B **73**, 125411 (2006).
[19]A. H. Castro Neto, N. M. R. Peres, K. S. Novoselov, and A. K. Geim, Rev. Mod. Phys. **81**, 109 (2009).
[20]H. C. Cheng, R. J. Shiue, C. C. Tsai, W. Hua Wang, and Y. T. Chen, ACS Nano **5**, 2051 (2011).
[21]B. Oziyilmaz, P. Jarillo-Herrero, D. Efetov, D. A. Abanin, L. S. Levitov, and P. Kim, Phys. Rev. Lett. **99**, 166804 (2007).
[22]M. I. Katsnelson, K. S. Novoselov, and A. K. Geim, Nat. Phys. **2**, 620 (2006).
[23]V. V. Cheianov, V. Falko, and B. L. Altshuler, Science **315**, 1252 (2007).
[24]Z. Wu, Appl. Phys. Lett. **98**, 082117 (2011).